Available online at www.sciencedirect.com
SCIENCE DIRECT®
ELSEVIER
International Journal of Solids and Structures 43 (2006) 2378–2397
INTERNATIONAL JOURNAL OF SOLIDS and STRUCTURES
www.elsevier.com/locate/ijsolstr

Numerical investigation of ductile tearing in surface cracked pipes using line-springs

K.R. Jayadevan [a,1], Espen Berg [a], Christian Thaulow [a,*], Erling Østby [b], Bjørn Skallerud [a]

[a] *Norwegian University of Science and Technology, Faculty of Engineering Science and Technology, 7491 Trondheim, Norway*
[b] *Sintef Material Technology, 7465 Trondheim, Norway*

Received 7 January 2005; received in revised form 19 June 2005
Available online 2 September 2005

Abstract

Accurate prediction of crack-driving force equations is important in any pipeline fracture assessment program. In highly ductile materials, such as pipeline steel, a considerable amount of stable crack growth can be tolerated before the failure of the structure. The existing methods use simplified analytical procedures to account for ductile tearing, and they often result in conservative critical crack sizes. Further, none of the published numerical tools for modelling crack growth is suitable for engineering applications. This work describes a simple method for simulating through-thickness ductile tearing in surface cracked pipes, using line-spring finite elements. The crack growth resistance curve is used to advance the crack front. The line-spring results are verified using crack growth simulations employing the Gurson damage model. Finally, a detailed parametric study is carried out to examine the effect of ductile tearing on crack driving force relationships in circumferentially surface cracked pipes. The results demonstrate that considering ductile tearing is important in fracture assessment procedures for pipelines.
© 2005 Published by Elsevier Ltd.

Keywords: Ductile crack growth; Surface cracked pipes; Line-spring method; Structural integrity

1. Introduction

Surface flaws such as welding defects, cracks and damage due to corrosion, etc., are common in girth welded offshore pipelines. For highly ductile materials such as pipeline steels, considerable amount of crack

* Corresponding author. Tel.: +47 73 593821; fax: +47 73 594129.
E-mail address: christian.thaulow@ntnu.no (C. Thaulow).
[1] Present address: Department of Mechanical Engineering, Government Engineering College, Thrissur, Kerala, India.

0020-7683/$ - see front matter © 2005 Published by Elsevier Ltd.
doi:10.1016/j.ijsolstr.2005.06.098

growth can be tolerated before the catastrophic failure of the structure. The present methodologies (for example BS7910:1999) for fracture assessment of pipelines employ simplified analytical procedures to include ductile tearing. This usually leads to stringent critical flaw size limits and excessive installation costs. A simple tool that can accurately predict crack-driving force relations in surface cracked pipes by simulating ductile tearing is demanded.

Several crack growth simulation procedures such as the Gurson model (Tvergaard and Needleman, 1984), the cohesive zone model (Besson et al., 2001), cell models (Xia and Shih, 1995), are published in the literature. However, these models require several model parameters to be identified, which is one of the main difficulties in applying them to structures. Further, these procedures are computationally expensive, and may cause numerical difficulties when applied to extensive problems, such as surface cracked pipes.

The line-spring finite element, initially proposed by Rice and Levy (1972) and later extended by Lee and Parks (1995), provides a simple approach to model surface cracks. Incorporating this line-spring technology, a new software, $\text{LINK}_{\text{pipe}}$ ($\text{LINK}_{\text{pipe}}$, 2003), that is tailormade for pipeline applications, has been developed using a co-rotated kinematic description of the ANDES shell and line-spring finite elements (Skallerud and Haugen, 1999; Skallerud, 1999). Numerical aspects and implementation of $\text{LINK}_{\text{pipe}}$ are described by Skallerud et al. (2005). Recently, Jayadevan et al. (2005) and Skallerud et al. (in press) have verified the accuracy of the line-spring method and its usefulness as an efficient computational tool for surface cracked pipes. An attractive feature of the line-spring element is that it easily facilitates the simulation of crack growth.

A ductile crack growth model using the line-spring finite element was proposed by Lee and Parks (1998a,b) for fully plastic, quasi-static through-thickness crack growth in surface cracked shell structures. They employed the plane-strain sliding-off and cracking model of McClintock et al. (1995) to obtain the instantaneous crack-tip opening angle in terms of the material parameters and the instantaneous slip-line angle and stress triaxiality at the crack-tip. However, this approach is not straightforward and it requires the determination of some model parameters from experiments. A more simplistic approach to propagate the crack in the line-spring model is to use the traditional material crack growth resistance curve. This is in accordance with the established use (BS7910:1999) of the resistance curve to account for ductile tearing. This also means that the constraint correction of the resistance curve (Nyhus et al., 2002) can be easily included in the simulations since the T-stress is readily available from the line-spring element.

The objective of this study is to demonstrate that line-spring finite element model is a simple and accurate procedure to investigate the ductile tearing in surface cracked pipes. The quasi-static stable crack growth is simulated using material tearing data. Since experimental ductile tearing data on surface cracked pipes is limited, the line-spring model is verified using continuum simulations of ductile crack growth. Using the line-spring model, a detailed parametric study on ductile tearing in surface cracked pipes along the through-thickness direction is performed. Then a range of crack depth and crack length values and diameter-to-thickness ratios of the pipe are considered under different loading conditions. The results show that the ductile tearing strongly influences the crack-driving force relations in surface cracked pipes. The study demonstrates the usefulness of parametric investigations in comparison to the underlying principles.

1.1. Line-spring theory

With the line-spring model, a surface cracked pipe is represented by a shell structure with a through slit. The stiffness from the ligament of the part-through crack is accounted for by introducing line-springs in the through slit, as schematically illustrated in Fig. 1. The local compliance of a spring connecting one point of the slit to the corresponding point on the other side is calculated based on known solutions of single edge notch (SEN) specimens under plane strain conditions. Thus, knowing the local compliance of a spring,

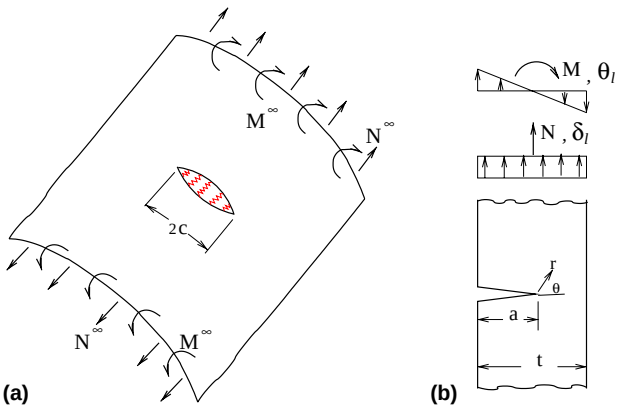

Fig. 1. (a) Shell model with line-springs representing a surface cracked pipe (see, Fig. 3). (b) The compliances at any point along the line-spring are obtained from a corresponding SEN bar in plane strain.

which depends on the crack depth along the crack front, we are able to calculate the stress intensity factor, K, the crack-driving force, J, and the crack tip opening displacement (CTOD).

1.1.1. Linear elastic line-spring element

When a cracked structure is analysed using the line-spring/shell model, the generalised shell stress resultants transmitted by the series of springs are a membrane force, N, and a bending moment, M, per unit length of the foundation. The work-conjugate deformation measures to these generalised resultants are the relative normal displacements, δ_L, and the relative rotation, θ_L. Denoting the membrane force, N, as Q_1 and the bending moment, M, as Q_2 and their work conjugate deformation measures as q_1 and q_2, the generalised forces and displacements are related in the elastic region by a compliance matrix, C_{ij}, as follows:

$$q_i = C_{ij}Q_j \quad (i,j = 1,2), \tag{1}$$

where C_{ij}, is determined from the stress intensity calibrations of SEN specimens using the energy/compliance relationship proposed by Rice (1972).

Using the generalised forces, the Mode-I stress intensity factor is given by

$$K_I = k_i(a,t)Q_i, \tag{2}$$

where $k_i(a,t)$ are functions that can be obtained, e.g., from the fracture handbook by Tada et al. (1985). The J-integral is then related to the stress intensity factor, in the case of plane strain, by the equation,

$$J = (1-\nu^2)\frac{K_I^2}{E}, \tag{3}$$

where E is Young's modulus and ν is Poisson's ratio of the material in consideration.

Similarly, T-stress at any point along the crack-front can be expressed as (Wang and Parks, 1992)

$$T = g_i(a,t)Q_i, \tag{4}$$

where functions g_i are calibration factors for T in an SEN specimen (Sham, 1991) with the same crack depth $a(s)$ and width t, under unit membrane and bending loads.

1.1.2. Elastic–plastic crack growth line-spring element

The fully plastic response of the line-spring model is based on a convex yield function, $\Phi\{Q_i; a, t; \sigma_y(\varepsilon^p)\}$, where $\sigma_y(\varepsilon^p)$ is the current uniaxial yield stress at an equivalent plastic strain of ε^p (Rice, 1972; Parks and White, 1982; Lee and Parks, 1995; Chiesa et al., 2002).

The Mode-I, elastic–plastic crack growth behaviour of the line-spring model assumes an incremental formulation based on a simple associated flow rule. The yield surface expands due to material hardening whereas it contracts during crack growth. In the present line-spring model, the crack growth is fully plastic, and the crack is propagated quasi-statically based on the material tearing data.

The incremental elastic–plastic line-spring formulation assumes an additive decomposition of the total generalised displacement increments, Δq_i, into elastic and plastic parts, i.e., $\Delta q_i = \Delta q_i^e + \Delta q_i^p$. The elastic part of the generalised displacement increment is related to the generalised force increment, ΔQ, through the elastic compliance matrix, C_{ij}, as follows:

$$\Delta q_i^e = C_{ij} \Delta Q_j. \tag{5}$$

The plastic part of the generalised displacement increment that is assumed to satisfy the normality rule, is taken to be the product of a positive scalar quantity, Λ, and the outward normal to the yield surface. Thus,

$$\Delta q_i^p = \Lambda \frac{\partial \Phi}{\partial Q_i}. \tag{6}$$

The scalar Λ is determined from the consistency condition

$$\dot{\Phi}(Q_i; a, t; \sigma_y) = 0. \tag{7}$$

The new crack length at the end of a time increment is expressed as

$$a^{(i+1)} = a^{(i)} + \Delta a^{(i)}, \tag{8}$$

where i denotes the time step and $\Delta a^{(i)}$ is the incremental crack growth during the ith step. This incremental crack advance is predicted from the material crack growth resistance curve.

In order to relate the plastic part of the generalised incremental displacement, Δq_i^p, and the incremental ligament-average plastic strain, $\Delta \varepsilon_y^p$, which directly follows the stress–strain data of the material, the plastic work increment per unit length of the flaw, ΔW^p is expressed in two different ways. Using the generalised field quantities, ΔW^p may be written as,

$$\Delta W^p = Q_i \Delta q_i^p, \tag{9}$$

and in terms of the uniaxial field quantities over the area A of the SEN specimen where plastic dissipation occurs as,

$$\Delta W^p = \int_A \sigma_y(\varepsilon^p) \Delta \varepsilon_y^p \, \mathrm{d}A. \tag{10}$$

Parks (1981) reasoned that the plastic dissipation area A for a deep crack is proportional to the square of the remaining ligament $(t - a)$, and for shallow cracks this area A is proportional to the square of a characteristic length, which is still related to $(t - a)$. Then, following Parks (1981), the above integral can be approximated as,

$$\Delta W^p = f \sigma_y(\varepsilon^p) \Delta \varepsilon_y^p (t - a)^2, \tag{11}$$

where the dimensionless scalar f is expected to be of order unity. Now, the assumption of equivalence of macroscopic (Eq. (9)) and continuum (Eq. (10)) plastic work increments completes a set of incremental constitutive relations for elastic–plastic hardening behaviour of the line-spring model.

The crack-driving force J as well as crack-tip opening displacement δ_t is divided into elastic and plastic parts, J^e and J^p and δ^e and δ^p. The elastic part of the driving force is calculated using Eq. (3). ASTM E 1290 suggests that the elastic part of CTOD of a hardening material in plane strain small scale yielding conditions can be estimated as

$$\delta^e = \frac{J^e}{m\sigma_y}, \tag{12}$$

where m is a scalar. In ASTM E 1290, a value of 2.0 for m is suggested. The plastic part of CTOD is related to the plastic parts of the load point displacement (δ_l^p) and rotation (θ_l^p) in incremental form (Lee and Parks, 1995) as

$$\Delta\delta^p = C_1(Q_i, \sigma_y, a/t)\Delta\delta_l^p + C_2(Q_i, \sigma_y, a/t)t\Delta\theta_l^p, \tag{13}$$

where the dimensionless functions C_i, are discussed by Lee and Parks (1995).

In principle, the evaluation of T-stress (Eq. (4)) can be extended to elastic–plastic deformation, using the current values of the membrane and bending forces. Recently, Jayadevan et al. (2005) showed that at large plastic strain levels, such "elastic–plastic" T-stress better quantifies the constraint level than the elastically computed T-stress.

2. Modelling aspects

2.1. An edge cracked plate

A single edge notched tension specimen (SENT) under plane strain assumptions is modelled using shell/line-spring as well as continuum elements as a benchmark problem for the line-spring crack growth model. Also, these continuum analyses provide the crack growth curves which are used to propagate the crack in the line-spring models. A width of 20 mm and a total length of 400 mm are selected for the SENT model. Different crack depth-to-width ratios of 0.1–0.5 are considered.

Two-dimensional, plane strain, 4-node quadrilateral elements are employed for the continuum model. The smallest element size near the crack tip is 0.1 mm. The effects of finite strains are accounted in these analyses. The material is assumed to be composed of a ductile matrix with micro-voids. The complete Gurson model (CGM) proposed by Zhang et al. (2000) is employed to simulate the ductile crack growth. In this model, the critical void volume fraction is not a constant but is predicted by the attainment of Thomason's plastic limit load criteria (Thomason, 1990). A typical initial void volume fraction of 0.001 is considered (Chen and Lambert, 2003). Other Gurson parameters are chosen to be the same as those suggested by Chen and Lambert (2003). The uniaxial plastic behaviour of the matrix material follows the isotropic power law hardening in the following form:

$$\frac{\sigma_y}{\sigma_0} = \left(1 + \frac{\varepsilon^p}{\varepsilon_0}\right)^n, \quad \text{for } \sigma_y > \sigma_0 \tag{14}$$

where σ_0 and $\varepsilon_0 = \sigma_0/E$ denote the initial yield stress and strain, respectively. Further, n is the hardening exponent. The behaviour is elastic for $\sigma_y < \sigma_0$. The yield strength, hardening exponent, Young's modulus, Poisson's ratio of the matrix material are taken as 460 MPa, 0.07, 200 GPa, 0.3 (typical of X65 pipeline steel). The continuum analyses were carried out using the ABAQUS (2003) finite element program. CGM was implemented into the ABAQUS finite element code through the user subroutine UMAT.

The line-spring model comprises a row of 4-node shell elements and a single line-spring element to model the crack. Plane strain conditions were simulated through appropriate boundary conditions. One end of the specimen was fixed whereas the other end was specified with prescribed axial displacements. The material

properties were assumed to be the same as those for the matrix material in the continuum model. The crack growth curves predicted from the Gurson simulations were used as the input to the line-spring model to propagate the crack.

2.2. A surface cracked pipe

The details of the pipe geometry considered in this work are shown in Fig. 2. An external surface cracked long straight pipe with outer diameter, D, and wall thickness, t, chosen for the simulations is shown in Fig. 2(a). For simplicity, the crack is assumed to be of uniform depth, a, along the circumferential crack length, $2c$, with an end-radius equal to the crack depth. Moreover, this crack geometry represents well the weld defects commonly observed in offshore pipelines. The details of the crack geometry are shown in Fig. 2(b). Further, the crack is symmetrically positioned on the pipe with respect to all the three axes as shown in the figure.

Two different loading cases, pure tensile loading and bend loading are considered. The effect of additional internal pressure along with tensile load is also investigated. Different diameter-to-thickness ratios ($D/t = 10$–50), crack depth to thickness ratios ($a/t = 0.1$–0.5), and crack length to perimeter ratios ($c/\pi R = 0.05$–0.3) are chosen. A fixed wall thickness, t, of 20 mm is employed in the simulations. In all the analyses, the total length, $2L$ of the pipe segment is chosen to be six times the outer diameter. Earlier studies (Jayadevan et al., 2004a; Østby et al., 2005) have shown that a length of 6D is sufficient to minimise the end-effects due to loading.

The line-spring model of the surface cracked pipe comprises 31 4-node shell elements along the length ($2L = 6D$). Depending on the flaw length, 12–24 line-spring elements are used to model the crack ($0.05 < c/\pi R < 0.3$), and correspondingly 30–42 shell elements along the circumferential direction of the pipe model. The end-radius of the crack-front was not modelled, instead a uniform crack depth along the length of the crack was specified. Our recent studies (Jayadevan et al., 2005) have shown that the end-radius of the crack front has negligible influence on the fracture parameters for most other parts of the crack. For convenience, the whole pipe is modelled irrespective of symmetry in the line-spring/shell models. A typical mesh used in the analyses is shown in Fig. 3(a). For tensile loading, one end of the pipe with fixed boundary and at the other end a prescribed displacement was employed. In the case of bend loading, a prescribed rotation was specified at both the ends. Also, the deformation at the end of the pipe is

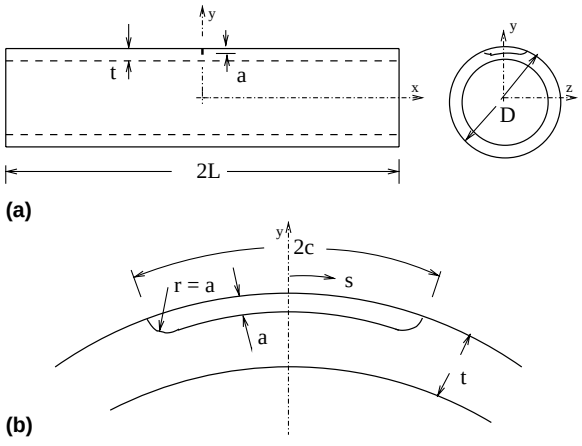

Fig. 2. (a) Geometry of the pipe with an external circumferential surface flaw and (b) details of the surface crack.

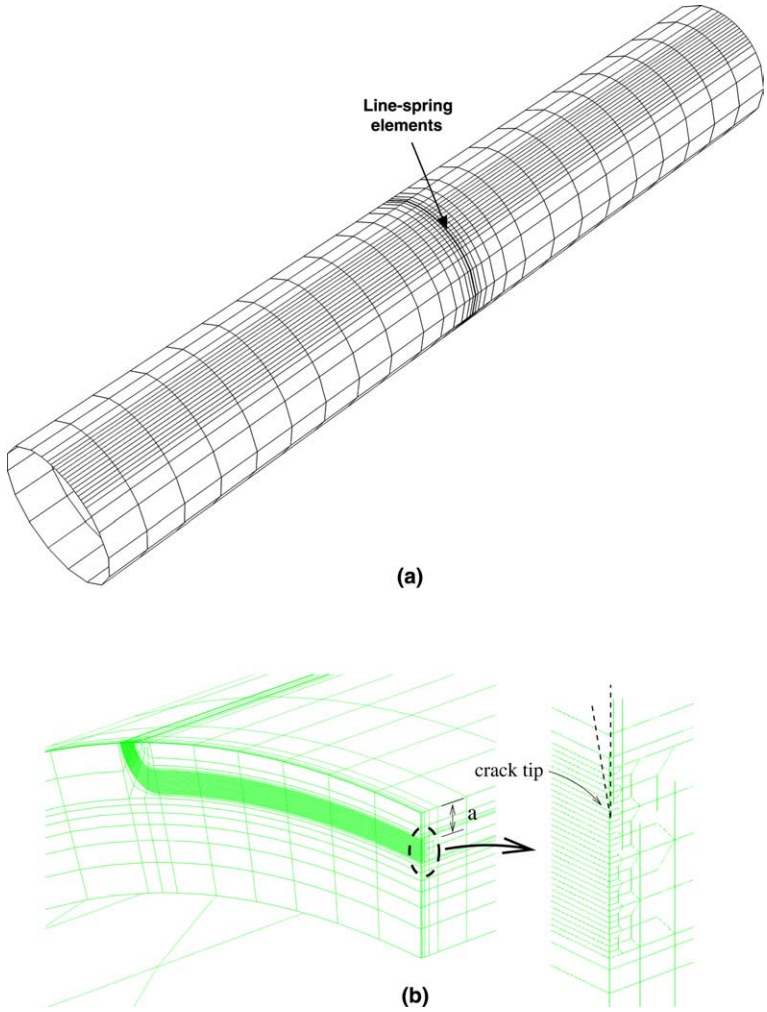

Fig. 3. (a) A typical finite element mesh used for the line-spring model ($c/\pi R = 0.1$, $a/t = 0.2$, $D/t = 20$) and (b) the near tip region of the 3D model employed to simulate ductile crack growth.

constrained in a plane. The same material properties as in the SENT simulations were used for pipes. Also, the crack growth curves obtained from the respective 2D continuum analyses of edge cracked specimens were employed for the surface cracked pipes with corresponding crack depths.

For comparison, the ductile crack growth for a typical case ($a/t = 0.2$, $c/\pi R = 0.1$, $D/t = 20$) was also simulated using a 3D model. In this case, numerical difficulties were experienced due to excessive mesh distortion near the crack-tip while using the CGM model. Hence, the Gurson model without any failure criterion was used as implemented in ABAQUS (2003) for static analyses. This model does not account for the void coalescence and faster void growth after a critical stage. However, it is expected to reasonably capture the ductile tearing response as predicted by the CGM model. Only a quarter of the pipe was modelled for the 3D analysis. 4032, 20-node brick elements (C3D20R in ABAQUS) with 19005 nodes were used under reduced integration. The smallest element size near the crack-tip was fixed at 0.1 mm. The near tip region of the mesh is shown in Fig. 3(b). The effects of finite strains were also accounted in this analysis.

3. Numerical results

3.1. Validation of line-spring calculations

3.1.1. SENT specimen

The crack growth resistance curves obtained from the 2D continuum simulations of SENT specimens are shown in Fig. 4. The variation of crack-tip opening displacement (CTOD) with accumulated total crack growth are presented for different initial crack depths. It can be noticed from this figure that as the initial crack depth decreases (i.e., less constraint), the CTOD value at any given crack growth increases, raising the resistance curves for the shallow specimens above the variations for deep cracked specimens. This is more pronounced for the shallowest crack (see Fig. 4). Also, the ductile crack initiation values are found to increase with the decrease in crack depth. Thus, Fig. 4 shows that the CTOD at initiation for the shallowest crack ($a/t = 0.1$) is about 0.45 mm whereas the same for the deepest crack ($a/t = 0.5$) is only about 0.21 mm. The results demonstrate that the resistance curve is not a material property alone, but depends also on the geometry, which has also been observed in experimental studies (Nyhus et al., 2002). Further, the experimental data by Nyhus et al. (2003) also indicate a similar effect of constraint on ductile crack initiation values as observed in the present simulations. The resistance curves presented in Fig. 4 are used as the input to the crack growth line-spring model to propagate the crack.

The evolution of CTOD and load versus the nominal strain for a SENT specimen ($a_0/t = 0.2$) are presented in Fig. 5(a) and (b), respectively. The load is normalised with respect to the limit load for an uncracked plate of unit width ($P_L = t\sigma_0$). The ductile tearing results obtained from both continuum (legend as "2DC-CG") and line-spring (legend as "LS-CG") models are displayed in these figures. Also, the results obtained from the analyses of the same specimens assuming a stationary crack are included for comparison. These results from the continuum and line-spring simulations of the stationary crack are marked in Fig. 5 as "2DC-ST" and "LS-ST", respectively.

In general, the results in Fig. 5(a) and (b) show that the local and global responses for both crack growth and stationary cases from the line-spring model agree reasonably well with those from the continuum analyses. Considering the evolutions of CTOD shown in Fig. 5(a), as the crack starts to grow, the CTOD increases more rapidly with nominal strain compared to the stationary case. On the global response, ductile tearing causes the load to drop first gradually and later rapidly from the stationary case (see Fig. 5(b)). Fig. 5(a) and (b) reveal that the crack growth line-spring element slightly overestimates the CTOD

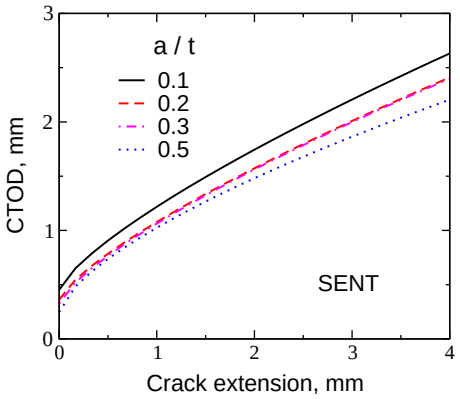

Fig. 4. The crack growth resistance curves for the SENT specimens corresponding to different crack depths as predicted by the Gurson model.

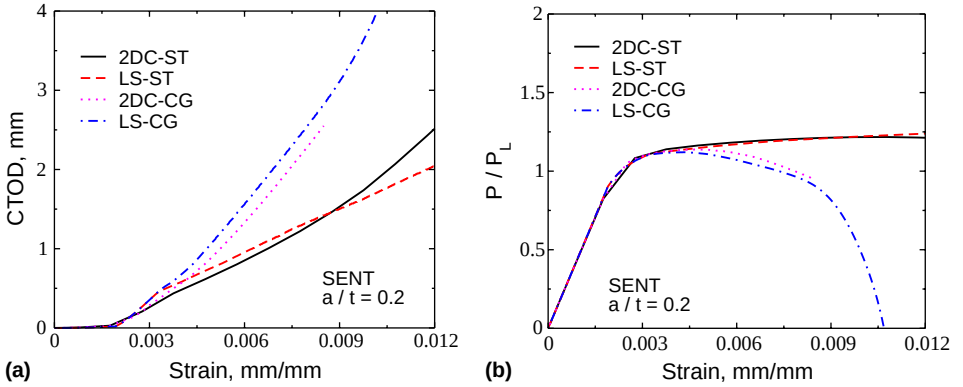

Fig. 5. The local and global responses predicted from the continuum (“2DC”) and line-spring (“LS”) crack growth (“CG”) models for the SENT specimen with $a/t = 0.2$. The results from the stationary crack (“ST”) are also included for comparison.

compared to the continuum results. On the other hand, the corresponding load response is slightly underestimated. Thus, the line-spring model appears to have a slightly higher crack growth rate than that in the continuum model. The slight deviations between the continuum and line-spring results may be attributed to the fact that the line-spring yield surfaces during crack growth are interpolated from the tabulated yield surfaces (Lee and Parks, 1995). The interpolated yield surface may drift slightly from the actual yield surface. Further, it may be noted that the present line-spring element does not account for the ligament necking observed at large strains. However, it is worth mentioning that the deviations of both CTOD and load during ductile tearing predicted from the line-spring model are on the conservative side.

3.1.2. A cracked pipe

Next, the ductile crack growth in a surface cracked pipe ($a_0/t = 0.2$, $c/\pi R = 0.1$, $D/t = 20$) under tensile loading is considered for the validation. The results showing CTOD (at $s = 0$) and global load versus applied nominal strain predicted by the line-spring and 3D models are presented in Fig. 6(a) and (b), respectively. The load is normalised with respect to the limit load for the uncracked pipe ($P_L = \pi(D - t)t\sigma_0$). For

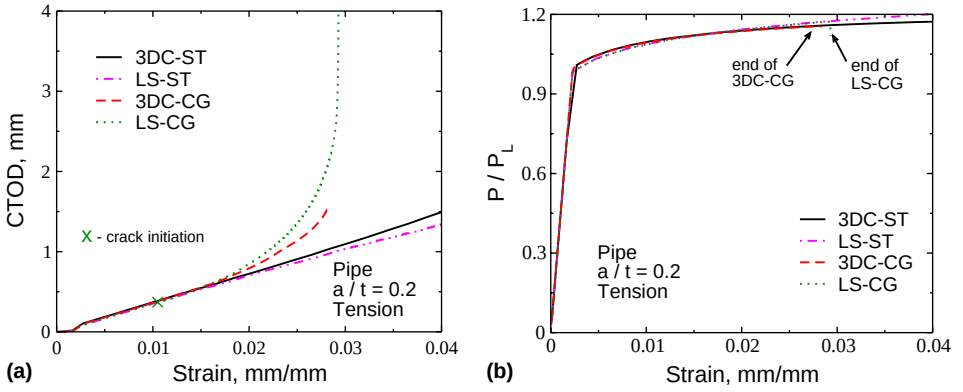

Fig. 6. A comparison of ductile crack growth responses in a surface cracked pipe ($a/t = 0.2$, $c/\pi R = 0.1$, $D/t = 20$) under tension as predicted from the crack growth line-spring and 3D damage models. The variations of (a) CTOD and (b) global load with nominal strain. Results from simulations assuming a stationary crack are also included.

comparison, the results for the stationary crack are also included in this figure. The legends in Fig. 6 are marked in a similar manner as in Fig. 5. The initiation of crack growth in the line-spring model is marked as an "x" in Fig. 6(a). Also, for clarity, final points on the load response curves from crack growth simulations are denoted by arrows in Fig. 6(b).

Fig. 6(a) indicates that ductile tearing significantly influences the crack-driving force relationships in surface cracked pipes. For a stationary crack, the evolution of CTOD with deformation is more or less linear (Jayadevan et al., 2004a), except at low deformation levels where plasticity is limited to the ligament. Before the initiation of crack growth (the cross symbol in Fig. 6(a)), the CTOD curves for the tearing and stationary cases are almost identical. After the initiation, Fig. 6(a) shows that, initially, the increase in CTOD due to crack growth is marginal, and the CTOD curve for tearing follows the stationary case. However, with further deformation, the increase in CTOD due to ductile tearing becomes rapid, and the curve starts to deviate significantly from the stationary case. At a later stage, the CTOD increases rapidly with deformation showing the end of a stable crack growth regime.

Unlike the edge cracked specimen, the variations of load with strain as displayed in Fig. 6(b) indicate that the global response of surface cracked pipes is marginally affected by the through-thickness stable ductile tearing. However, an abrupt drop in load is noticed during the unstable crack growth. This can be explained by the fact that for surface cracked pipes with moderate crack length ($c/\pi R < 0.3$), the crack depth has only a marginal effect on the global load (Jayadevan et al., 2004b), particularly for $a/t < 0.5$. Hence, during crack growth (in the thickness direction), the deviation of load response from that of the uncracked pipe will be minimal up to moderately large crack depths. However, the increase in crack depth results in higher CTOD values, which in turn lead to faster crack growth. Finally, this accelerated local deformation leads to unstable tearing through the ligament to form a through crack. This gives rise to a sudden drop in the load, which must approximately be equal to the reduction in area due to a through crack. After that the load response is expected to follow that of a through-cracked pipe. It is worth mentioning that in the line-spring simulations, several incremental steps are involved during the abrupt load drop due to unstable tearing, and at a magnified scale it follows a smooth curve. Most of the present crack growth line-spring simulations (presented subsequently) were stopped when the maximum tearing reached a current crack depth ratio of 0.7–0.8.

More importantly, the results shown in Fig. 6 demonstrate that the fracture response predicted from the crack growth line-spring model and 3D damage model are in reasonable agreement. The 3D Gurson analysis was stopped due to numerical convergence problems when the analysis reached almost the end of stable damage growth. However, the trend in the 3D result suggests that the unstable tearing is expected somewhat at the same strain levels in both 3D and line-spring models. For the stationary case, an excellent match between the crack-driving force relationships from line-spring and 3D models can be noted. However for extensive crack growth, the deviation of the line-spring result from the 3D variation becomes noticeable (see, Fig. 6(a)). Mainly, this may be attributed to the fact that the present 3D ductile tearing analysis (using the original Gurson model) does not account for the void coalescence, and so a slower damage growth rate is expected. On the other hand, the resistance curve used in the line-spring simulation was predicted based on the complete Gurson model. This model accounts for void coalescence by accelerating void growth after a critical void volume fraction predicted by the Thomason's limit load criteria. In the numerical implementation, when the void volume fraction reaches an ultimate value, the element is assumed to have failed and the load carrying capacity of the element is gradually reduced to zero. Hence, a slightly higher crack growth rate for the line-spring model is expected compared to the damage growth rate in 3D model.

It may further be noted that the present line-spring and shell elements are based on a small-strain/large rotation formulation whereas finite strain effects are accounted in the 3D simulations. However, the results for the stationary case show that up to a strain level of about 3%, the crack-driving force relationships from line-spring and 3D models are in excellent agreement. Thus, for this case ($a/t < 0.2$), the consideration of

ligament necking is not important at these deformation levels. Further, during ductile tearing large strain effects are not expected to significantly influence the results. Hence, it is concluded that the crack growth line-spring model is a simple and accurate procedure for the simulation of ductile tearing in surface cracked pipes. However, it must be noted that for deep cracks, the ligament necking may begin at lower strain levels (see Section 4). The biaxial loading also enhance the ligament necking (Jayadevan et al., 2004a).

3.2. Parametric study

The effect of crack geometry, pipe geometry and loading conditions on the ductile tearing response of surface cracked pipes is examined using the crack growth line-spring model. Mainly, the local (CTOD) and global (load) responses are plotted versus the nominal strain. For comparison, results corresponding to the stationary crack are included for some cases.

3.2.1. Effect of crack depth

The CTOD versus deformation during ductile tearing in a surface cracked pipe ($c/\pi R = 0.1$ and $D/t = 20$) under tension are displayed in Fig. 8, respectively. The results corresponding to different crack depths are included in these figures. For the cases with $a/t = 0.2$ and 0.3, the results from the analyses of a stationary crack are plotted as thin lines to provide a direct comparison.

The local responses displayed in Fig. 7(a) show that for any given strain level the CTOD increases with an increase in crack depth. Hence, the crack growth initiates at lower levels of deformation as initial crack depth increases. Thus, while the ductile tearing in the shallowest ($a_0/t = 0.1$) crack starts at about 4% strain, the same ductile tearing at the deepest crack ($a_0/t = 0.5$) begins at strain levels below the yield strain. Further, as the initial crack depth increases, the stable crack growth regime becomes shortened and unstable tearing starts at lower levels of deformation. Thus, the unstable ductile tearing in the deepest cracked pipe occurs almost just after the initiation, and stable crack growth is only marginal.

When comparing the CTOD responses for the stationary and tearing cases ($a/t = 0.2$ and 0.3), it can be seen that ductile tearing significantly decreases the deformation capacity of the pipe. It must be noted that the present line-spring element does not account for ligament necking, and hence the linear CTOD-strain relationship for stationary cracks extends up to large strain levels. However assuming a stationary crack detailed 3D finite element simulations (Jayadevan et al., 2004a) for surface cracked pipes have shown that for large strain levels, a rapid increase in CTOD with strain occurs after a certain deformation level due to

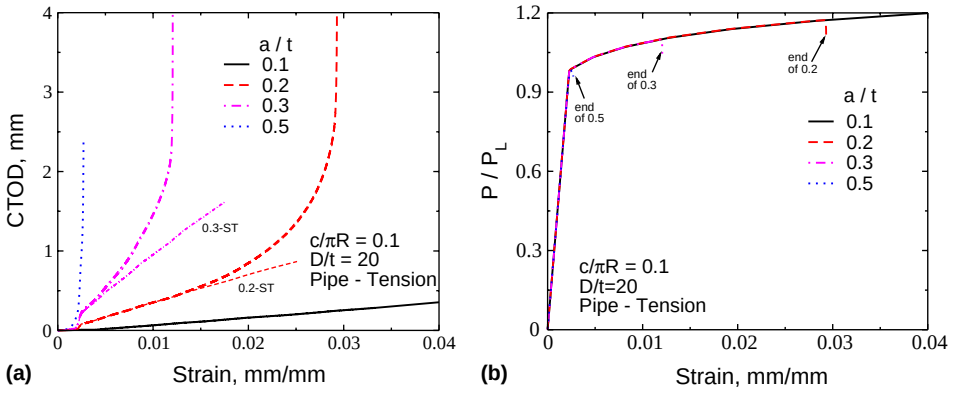

Fig. 7. The effect of crack depth on ductile tearing in surface cracked pipes ($c/\pi R = 0.1$ and $D/t = 20$) under tension as predicted from the crack growth line-spring model. Variations of (a) CTOD and (b) global load with nominal strain.

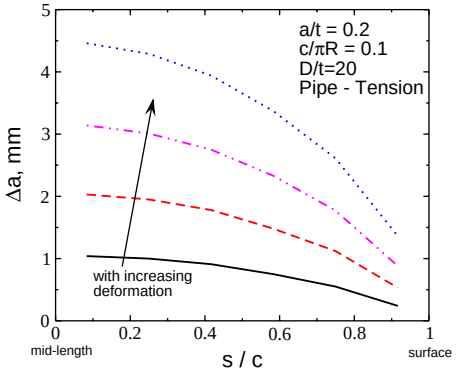

Fig. 8. Ductile crack growth along the crack-front predicted from the line-spring model for a surface cracked pipe ($a/t = 0.2$, $c/\pi R = 0.1$ and $D/t = 20$) under tension, corresponding to different deformation levels.

ligament necking and enhanced local deformation. This deformation level at which a rapid increase in CTOD occurs, decreases with an increase in crack depth. For the stationary case with $a/t = 0.2$ and 0.3 (see Section 4), the effect of ligament necking becomes significant after a strain level of about 3.0% and 1.7%, respectively. Hence, for deep cracks ($a/t > 0.2$) consideration of ligament necking may further enhance the increase in CTOD with deformation during stable crack growth and it may slightly decrease the deformation capacity from the present line-spring predictions. In general, the results demonstrate that consideration of ductile tearing is important in the fracture assessment procedures for moderately deep ($a/t > 0.1$) surface cracked pipes.

The normalised global load response for the same cases as in Fig. 7(a) is displayed in Fig. 7(b). The load is normalised with respect to the limit load ($P_L = \pi(D - t)t\sigma_0$) for the uncracked pipe. These results also illustrate that the ductile tearing significantly reduces the deformation capacity of surface cracked pipes. During stable tearing the load, response is marginally affected by crack depth. However, when unstable tearing starts, the load drops abruptly. It is expected that the load will continue to drop till the tearing covers the entire ligament to form a through-crack. Fig. 7(b) shows that for deep cracks, the load capacity of the pipe also becomes reduced by ductile tearing. Thus, for the deepest crack, the maximum load is about the load at which global yielding of the pipe starts.

The crack growth along the crack front for the case with $a_0/t = 0.2$ is displayed in Fig. 8. The results are presented for different deformation levels. These results show that the ductile tearing is more or less uniform over 50–60% of the crack length from the mid-section, particularly at low deformation levels. Near the free surface, crack growth is less compared to that at the mid-section. At large deformation levels, the variation of tearing along the crack is more pronounced. The experimental ductile tearing studies (Nyhus et al., 2002) on sector SENT specimens prepared from an X65 pipe also show a similar variation of crack growth along the width of the specimen.

3.3. Effect of crack length

The local and global responses showing the effect of crack length on ductile tearing are displayed in Fig. 9(a) and (b), respectively. These results correspond to a surface cracked pipe with $a_0/t = 0.2$ and $D/t = 20$ under tension. For comparison, the results for the stationary cases ($c/\pi R = 0.1$ and 0.3) are also plotted in this figure as thin lines. The CTOD-strain variations shown in Fig. 9(a) illustrate that before the initiation of crack growth, only a marginal increase in CTOD is observed with the increase in crack length. However, after the initiation of ductile tearing a significant increase in CTOD at any given strain level may

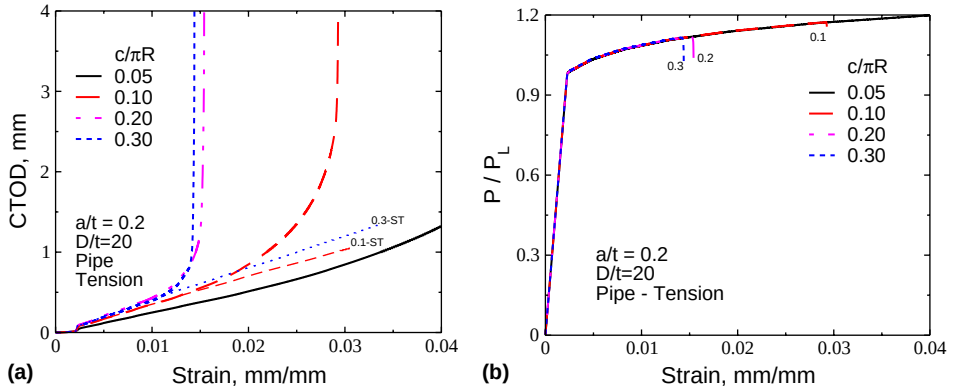

Fig. 9. The effect of crack length on ductile tearing in surface cracked pipes ($a/t = 0.2$ and $D/t = 20$) under tension as predicted from the crack growth line-spring model. Variations of (a) CTOD and (b) global load with nominal strain.

be noted. Further, as the crack length increases, the strain level at which unstable tearing starts decreases significantly. Thus, while the unstable ductile tearing for the shortest crack ($c/\pi R = 0.05$) starts above 4% strain, for the longest crack ($c/\pi R = 0.3$) this is below 1.5%. Fig. 9(a), further shows that the effect of crack length on CTOD-strain response is less pronounced for long cracks. Finally, the results demonstrate that unlike the stationary case, the CTOD-strain relationship for surface cracked pipes depends strongly on the crack length during ductile tearing.

The reduction in deformation capacity can be clearly noticed from the normalised load responses as displayed in Fig. 9(b). The effect of crack length on the load response curve is marginal during stable tearing. However, when unstable tearing of the ligament begins, the load starts to decrease abruptly. The decrease in deformation capacity with increase in crack length is more pronounced for short cracks. Thus, as the crack length ratio $c/\pi R$ changes from 5% to 10%, the deformation capacity decreases by about 40%. On the other hand, the corresponding change in deformation capacity for the increase in $c/\pi R$ from 20% to 30% is only marginal (<5%).

3.4. Effect of diameter-to-thickness ratio

In Fig. 10(a) and (b), the CTOD and load variations during ductile tearing of cracked pipes with different diameter-to-thickness ratios are presented. These results correspond to a surface cracked pipe with $a_0/t = 0.2$ and $c/\pi R = 0.1$ under tensile loading. The CTOD results for the stationary cases corresponding to $D/t = 20$ and 40 are plotted in Fig. 10(a) as thin lines.

The evolutions of CTOD shown in Fig. 10(a) illustrate that when ductile tearing is accounted for, the D/t ratio of surface cracked pipes strongly affects the crack-driving force relationships. Before the initiation of ductile tearing, the effect of D/t on CTOD-strain relationship is marginal which agrees with the observations reported by Jayadevan et al. (2004a). However, after the crack growth is initiated, the CTOD at any given strain level increases with increase in D/t. Also, the unstable crack growth in higher diameter pipes occurs at lower strain levels compared to those for lower D/t cases. Thus, while the unstable tearing for the lowest diameter pipe ($D/t = 20$) starts at about 3% strain level, the same for the highest diameter pipe ($D/t = 50$) is 1.6%. On comparing the stationary and tearing results, it can be seen that the consideration of ductile tearing becomes more important for thin pipes.

The reduction in deformation capacity due to unstable tearing can be clearly noticed from the global load responses shown in Fig. 10(b). During stable ductile tearing, the normalised global load is only marginally affected by the diameter-to-thickness ratio.

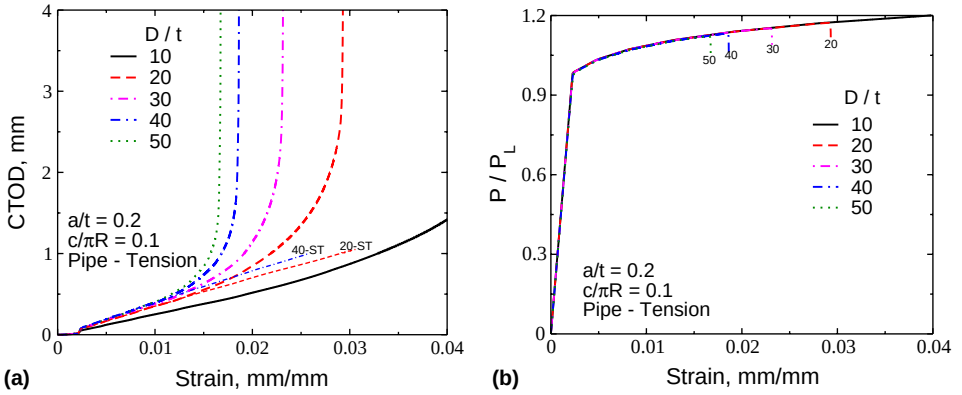

Fig. 10. The effect of diameter-to-thickness ratio on ductile tearing in surface cracked pipes ($a/t = 0.2$ and $c/\pi R = 0.1$) under tension as predicted from the crack growth line-spring model. Variations of (a) CTOD and (b) global load with nominal strain.

3.5. Effect of biaxial loading

Fig. 11 shows the results obtained from the tensile loading of a surface cracked pipe ($a/t = 0.2$, $c/\pi R = 0.1$ and $D/t = 20$) with additional internal pressure. The results corresponding to different magnitudes of internal pressure are included. The magnitude of pressure is marked as the ratio of hoop stress caused by the internal pressure to the initial yield stress (σ_h/σ_0). It may be recalled that the pressure load was applied first, and then the end displacements were applied gradually, since this loading sequence corresponds to realistic situations.

The CTOD responses displayed in Fig. 11(a) show that as the magnitude of hoop stress rises, the CTOD at any given strain level increases significantly. For stationary cracks, Jayadevan et al. (2004a) have verified from the 3D finite element analyses of surface cracked pipes that the ligament localisation is strongly enhanced by biaxial loading. Also, for the same deformation level, the biaxial loading increases the load carrying capacity of the ligament, which is also reflected in the global load response as shown in

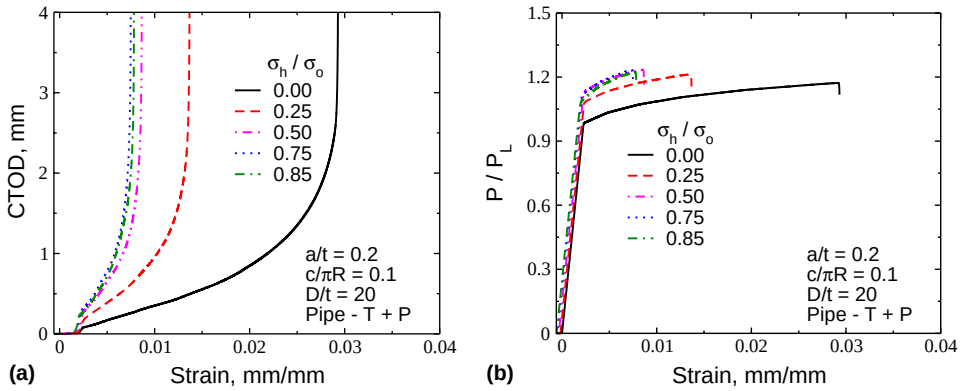

Fig. 11. The effect of biaxial loading on ductile tearing in a surface cracked pipe ($a/t = 0.2$, $c/\pi R = 0.1$ and $D/t = 20$) under tension as predicted from the crack growth line-spring model. (a) Variations of CTOD and (b) global load with nominal strain.

Fig. 11(b). This increased local loading for the same strain level leads to more enhanced local deformation, and hence, higher CTOD values under biaxial loading.

More importantly, Fig. 11(a) demonstrates that as the magnitude of internal pressure increases, the unstable tearing begins at lower deformation levels. In other words, the deformation capacity of the cracked pipe is significantly reduced under biaxial loading. This can clearly be seen from the global load responses (Fig. 11(b)). Thus, while the deformation capacity for pure tensile loading case is about 2.9%, the same for the case of $\sigma_h/\sigma_0 = 0.75$ is below 0.8%. Further, Fig. 11(a) and (b) illustrate that the effect of internal pressure on ductile tearing response is less pronounced at larger magnitudes of hoop stress.

3.6. Bend loading

In practice, the pipelines may also be subjected to bend loading with or without internal pressure. In order to examine the ductile tearing response under bending, some typical results are plotted in Fig. 12. The evolution of CTOD and normalised moment with nominal strain for two crack depths ($a_0/t = 0.2$ and 0.3) under pure bending of the pipe are displayed in Fig. 12(a) and (b), respectively. The nominal strain is computed from the average curvature over the whole length of the pipe ($\varepsilon = D\phi/2L$, ϕ being the prescribed rotation at the end of the pipe). The moment is normalised with respect to the limit moment for an uncracked pipe ($M_L = 4R^2t\sigma_0$, R being the mean radius of the pipe). The CTOD results from tensile loading is included in Fig. 12(a) for direct comparison.

The CTOD responses for pure bending shown in Fig. 12(a) illustrate that the crack-driving force variations during stable tearing are somewhat similar in bending and tension, as in the stationary case (Østby et al., 2005; Jayadevan et al., 2004b). However, for large crack growth, the CTOD values under tensile loading are higher than the corresponding results from bending. Also, for both crack depths, the values of deformation capacity predicted under tensile loading are slightly lower than those for bending.

The global moment responses displayed in Fig. 12(b) also show similar observations as in tensile loading (see Fig. 8(b)). Thus, the moment response is marginally affected during stable tearing, and later, when unstable tearing starts, the moment drops abruptly.

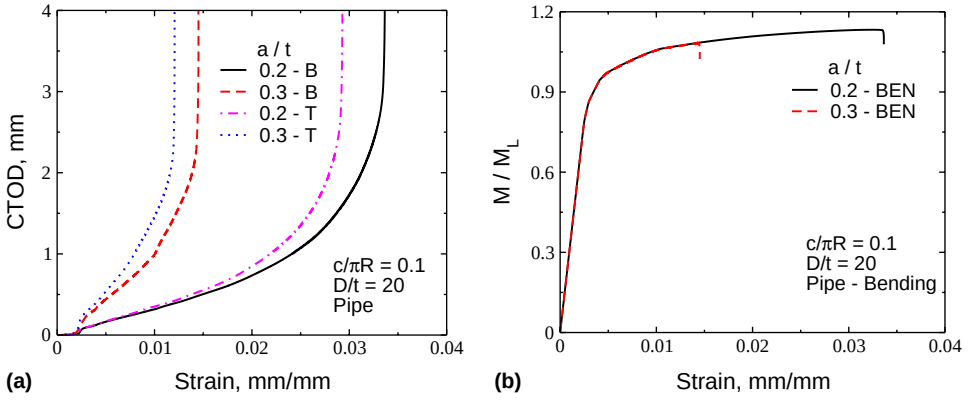

Fig. 12. The (a) CTOD and (b) normalised moment versus strain variations during ductile tearing in a surface cracked pipe ($c/\pi R = 0.1$ and $D/t = 20$) under pure bending for two different crack depths. For comparison the corresponding CTOD results from tensile analyses are plotted also in (a).

4. Discussion

Recently, a strain-based procedure for the fracture assessment of pipelines was proposed by Østby et al. (2005) and Jayadevan et al. (2004b). Based on detailed 3D finite element analyses of surface cracked pipes, a linear relationship for the variation of crack-driving force with deformation (CTOD-strain) was approximated as

$$\text{CTOD} = C_\delta \varepsilon. \tag{15}$$

Here, ε is the applied global strain and C_δ is a constant. C_δ is a function of crack and pipe geometry, internal pressure and material properties. Jayadevan et al. (2004a) noticed from their numerical results for stationary cracks that the function C_δ strongly depends on crack depth, magnitude of hoop stress and material properties. However, the influence of crack length and diameter-to-thickness ratio on C_δ was found to be less pronounced, particularly for cracks, $a/t < 0.3$.

On the other hand, the present tearing results demonstrate that once the tearing is initiated, the CTOD-strain relationship deviates from the linear approximation. Also, unlike the stationary case, both crack length and diameter-to-thickness ratio strongly influence the evolution of CTOD during tearing. For shallow cracks ($a_0/t < 0.1$), consideration of ductile tearing is not important since in this case the crack growth is unlikely to initiate even at a high strain level of 4%. In contrast, for cracks of $a_0/t > 0.1$, ductile tearing starts at lower strain levels, and it significantly reduces the deformation capacity from those predicted for stationary cracks. For example, under realistic loading situations of a surface cracked pipe with a crack depth of 4 mm ($a_0/t = 0.2$, see Fig. 11(a)) the deformation capacity is limited to less than 0.5% strain.

For highly ductile materials, initiation of crack growth may not be the limit for criticality. In practice, a significant amount of stable ductile crack growth can be tolerated prior to the failure. This consideration of ductile tearing can extend the allowable capacity of a cracked pipe as illustrated in Fig. 13. The CTOD-strain variation as predicted by crack growth line-spring element for a surface cracked pipe ($a/t = 0.2$, $c/\pi R = 0.1$ and $D/t = 20$) under tensile loading is replotted in Fig. 13. Also this figure plots the similar variations for a stationary crack of $a/t = 0.2$ and 0.3 predicted by line-spring and 3D simulations.

In fracture assessment procedures for ductile materials, a certain amount of ductile tearing is usually allowed depending on the crack growth resistance curve and nature of application. If we assume that 2 mm ductile crack growth is allowed, it follows from the corresponding resistance curve (see the curve for

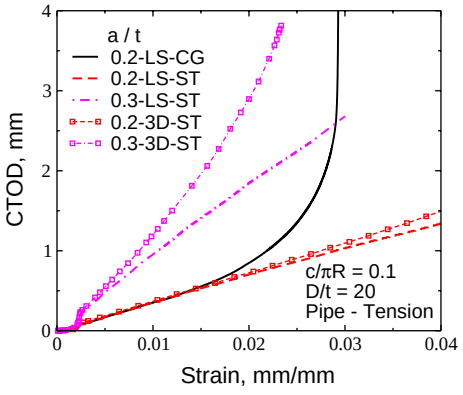

Fig. 13. The CTOD-strain variation during ductile tearing in a surface cracked pipe ($c/\pi R = 0.1$ and $D/t = 20$) under tension as predicted by line-spring model for $a/t = 0.2$. Similar results from line-spring and 3D simulations for stationary cracks with $a/t = 0.2$ and 0.3 are included for comparison.

$a_0/t = 0.2$ in Fig. 4) that the critical CTOD is about 1.6 mm. Also, assume that a 4 mm crack depth ($a_0/t = 0.2$) is the maximum undetected defect size during an inspection programme. Now, Fig. 13 shows that corresponding to this critical CTOD value of 1.6 mm, the strain level predicted by accounting for ductile tearing (the curve "0.2-LS-CG") is about 2.7%. On the other hand, the stationary line-spring model for $a_0/t = 0.3$ (the curve "0.3-LS-ST", 2 mm crack growth from $a_0/t = 0.2$ leads to $a_0/t = 0.3$) gives a deformation capacity of about 1.7%, whereas for $a_0/t = 0.2$ (the curve "0.2-LS-ST") this capacity is above 4%. Thus, the consideration of ductile tearing in surface cracked pipes can significantly extend the deformation capacity (about 1% in this case) from the stationary result. At the same time, accounting for ductile tearing reduces the maximum strain level by about half from that of the stationary case with the same initial crack depth. This demonstrates the importance of considering ductile tearing in the fracture assessment procedures for offshore pipelines.

It was mentioned that the present line-spring and shell elements are based on small-strain formulation, and hence, necking of the ligament under large deformation is not captured in these simulations. In order to illustrate the effect of finite strain, the CTOD-strain variations obtained from 3D finite element simulations of surface cracked pipes assuming a stationary crack are displayed along with the line-spring results in Fig. 13. The 3D results displayed with symbols account for finite strain effects. It may be noticed from these results that for $a_0/t = 0.2$, the line-spring results agree well with the 3D results up to a strain level of 2%. Later, the CTOD values from 3D simulation are higher than those from line-spring model. For $a_0/t = 0.3$, the deviation between the line-spring and 3D results starts at about 0.8% strain. Hence, the effect of large strain is important for moderately deep cracks ($a_0/t > 0.2$). The results for $a_0/t = 0.2$ demonstrate that there is marginal error in the present ductile crack growth results by not accounting for ligament necking.

It is well known that the crack growth resistance curve is not a material property but depends on the geometry or the stress triaxiality ahead of the crack tip (Nyhus et al., 2002). Recent experimental crack growth data for X65 steel reported by Storslett (2004) is replotted in Fig. 14(a). The crack growth resistance curves for single edge notched bend (SENB, $a/t = 0.2$ and 0.5) and tension (SENT, $a/t = 0.2$) specimens are displayed in this figure. These results clearly show the constraint effects on material-crack resistance curves. Thus, the resistance curve for deeply cracked SENB specimen which has the highest constraint falls below the other curves. On the other hand, the curve for the SENT specimen, which has the lowest constraint falls on the top. The present crack growth results (Fig. 4) for the SENT specimen as predicted using Gurson model also indicate that resistance curve changes with the constraint.

Nyhus et al. (2002) have shown that the resistance curves can be normalised based on elastic T-stress. They proposed that the resistance curves derived from different test specimens can be corrected for constraint based on a reference crack growth curve as,

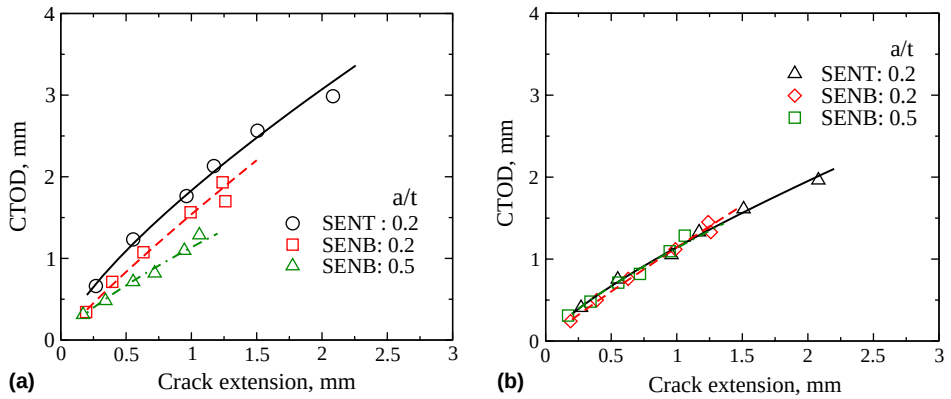

Fig. 14. (a) The experimental crack growth resistance curves and (b) constraint corrected resistance curves for X65 steel (Storslett, 2004).

$$\mathrm{CTOD}^{\mathrm{corr}} = \mathrm{CTOD}^{\mathrm{ref}} g(T). \tag{16}$$

Here, $\mathrm{CTOD}^{\mathrm{corr}}$ is the constraint corrected resistance curve and $\mathrm{CTOD}^{\mathrm{ref}}$ is the reference resistance curve. The term $g(T)$ is a geometry dependent function which may also depend on the material and temperature. Nyhus et al. (2002) employed the following function for $g(T)$, proposed initially by Ainsworth and O'Dowd (1994) for the constraint correction of resistance curve when applied to failure assessment diagrams:

$$g(T) = \left[1 + \alpha\left(-\frac{T(\Delta a)}{\sigma_0}\right)^m\right]^2 \quad \text{for } T < 0, \tag{17}$$

$$g(T) = 1 \quad \text{for } T \geqslant 0. \tag{18}$$

Here, α and m are constants which depend on the material. These constants can be determined from experimental resistance curves.

Storslett (2004) computed the value of α and m using the results shown in Fig. 14(a). He employed the data from deeply cracked SENB specimen as the reference resistance curve, and solved the unknown values of α and m using the other two crack growth curves (see Fig. 14(a)). In fact, Storslett (2004) has shown that in normalising the resistance curves, it is enough to calculate the function $g(T)$ at a particular value of crack growth. He computed the $g(T)$ function employing the CTOD values corresponding to a crack extension, $\Delta a = 1$ mm. The normalised resistance curves obtained using this function is displayed in Fig. 14(b). It can be clearly seen from this figure that the resistance curves can be well normalised by T-stress. As demonstrated by Jayadevan et al. (2005), this also indicates that the use of T-stress to quantify the constraint can be extended to large plastic strains.

The results shown in Fig. 14 demonstrate that the resistance curves can be constraint corrected, once the $g(T)$ function is available for that material. Generally, the T-stress needs to be computed as a function of crack growth. Usually, T-stress compendia (Sham, 1991; Sherry et al., 1995) are used for this purpose. However, the accuracy of such elastic T-stress under large plastic strains is questionable. For structural applications, T-stress has to be computed from separate analyses.

On the other hand, T-stress is readily available from the line-spring model. Recently, Jayadevan et al. (2005) have shown that an "elastic–plastic" T-stress can be computed from the line-spring element. In this case, the current values of membrane force and bending moment are used to compute the T-stress employing Eq. (4). Here, it is assumed that Eq. (4) is valid under plastic deformation. Jayadevan et al. (2005) have demonstrated that such "elastic–plastic" T-stress successfully quantifies the constraint level under large plastic deformation. This indicates the possibility of making constraint correction of the resistance curves while performing the actual analysis. This constraint correction has been implemented in the present line-spring program. A reference material resistance curve will be the input to the program. During each incremental crack growth step, the CTOD values from this reference curve will be modified according to the T-stress computed at that step from the line-spring element. Hence, the line-spring method provides a simple and accurate procedure for accounting for constraint effects while simulating ductile tearing in surface cracked pipes.

5. Concluding remarks

A crack growth line-spring model for simulating ductile tearing in surface cracked pipes is examined in this paper. Two- and three-dimensional analyses are carried out in order to verify the line-spring results. Using this line-spring model, a detailed parametric study is performed to investigate the effect of ductile tearing on crack-driving force relationships for surface cracked pipes. The main conclusions of this study are as follows:

- The ductile crack growth results from line-spring and detailed continuum simulations are in good agreement.
- Ductile tearing strongly influences the CTOD-strain relationships in surface cracked pipes. A significant reduction in deformation capacity from the stationary case is noticed when ductile tearing is considered. As initial crack depth increases, the effect of ductile tearing becomes more important.
- Unlike the stationary case, the crack length ratio strongly affects the CTOD-strain relationships during ductile tearing. With an increase in the crack length ratio, the deformation capacity decreases significantly.
- The effect of the diameter-to-thickness ratio of the pipe on CTOD-strain relationships during ductile tearing is very similar to that of the crack length.
- Under biaxial loading, a more pronounced effect of ductile tearing on the crack-driving force relationships is noted. With an increase in magnitude of internal pressure, the deformation capacity is reduced significantly. For a 4 mm cracked pipe with $a_0/t = 0.2$, a hoop stress loading of 50% of the yield stress reduces the strain capacity by about 83%.
- The global load response is marginally affected during stable ductile tearing. During unstable tearing the load drops abruptly.
- The ductile tearing response of surface cracked pipes under bending is very similar to that under tensile loading. Tensile loading gives slightly conservative estimates for the bending.
- This work demonstrates that the present crack growth line-spring model is a simple and accurate procedure for simulating ductile crack growth in surface cracked pipes.

It may also be mentioned that this study is focused on the through-thickness ductile crack growth of the circumferential surface crack. There can be situations in which a surface crack may also grow along the length before or during the through-thickness tearing. In these cases, other crack growth models (for example, cohesive zone model) may be combined with the line-spring method to simulate the ductile crack growth along both the thickness and length directions. Finally, it must be noted that the tearing curve has only physical meaning for small but finite extensions, and hence its use for large crack growth may not be theoretically appropriate.

Acknowledgements

The authors gratefully acknowledge the support from the Joint Industry Project ''Fracture Control Offshore Pipelines''. Also the first author would like to thank the Research Council of Norway for the financial support towards his research programme. The authors also thank Kjell Holthe, Faculty of Engineering Science and Technology, NTNU, Trondheim, Norway and Bård Nyhus and Lars Storslett, Sintef Materials Technology, Trondheim, Norway for valuable discussions during this work.

References

ABAQUS, 2003. Theory Manual, Version 6.3, Hibbit, Karlsson and Sorensen, Inc., Providence, RI.

Ainsworth, R.A., O'Dowd, N.P., 1994. A framework for including constraint effects in the failure assessment diagram approach for fracture assessment. In: Proceedings of ASME Pressure Vessels and Piping Conference, PVP-vol. 287/MD-vol. 47.

Besson, J., Steglich, D., Brocks, W., 2001. Modeling of crack growth in round bars and plane strain specimens. International Journal of Solids and Structures 38, 8259–8284.

BS7910:1999. Incorporating Amendment No. 1. Guide on methods for assessing the acceptability of flaws in metallic structures. British Standards Institute, 2000.

Chen, Y., Lambert, S., 2003. Analysis of ductile tearing of pipeline-steel in single edge notch tension specimens. International Journal of Fracture 124, 179–199.

Chiesa, M., Skallerud, B., Gross, D., 2002. Closed form line spring yield surfaces for deep and shallow cracks: formulation and numerical performance. Computers and Structures 80, 533–545.

Jayadevan, K.R., Østby, E., Thaulow, C., 2004a. Fracture response of surface cracked pipes under large deformations under tension. International Journal of Pressure Vessels and Piping 81, 771–783.

Jayadevan, K.R., Østby, E., Thaulow, C., 2004b. Strain-based fracture mechanics analysis of pipelines. In: Proceedings of International Conference on Advances in Structural Integrity, July 14–17, Indian Institute of Science, Bangalore, India.

Jayadevan, K.R., Thaulow, C., Østby, E., Berg, E., Skallerud, B., Holthe, K., Nyhus, B., 2005. Structural integrity of pipelines: *T*-stress by line-spring. International Journal of Fatigue and Fracture of Engineering Materials and Structures 28, 467–488.

Lee, H., Parks, D.M., 1995. Enhanced elastic–plastic line-spring finite element. International Journal of Solids and Structures 32, 2393–2418.

Lee, H., Parks, D.M., 1998a. Line-spring finite element for fully plastic crack growth—I. Formulation and one-dimensional results. International Journal of Solids and Structures 35, 5115–5138.

Lee, H., Parks, D.M., 1998b. Line-spring finite element for fully plastic crack growth—II. Surface cracked plates and pipes. International Journal of Solids and Structures 35, 5139–5158.

$LINK_{pipe}$, 2003. Verification manual, $LINK_{ftr}$, Trondheim, Norway.

McClintock, F.A., Kim, Y.-J., Parks, D.M., 1995. Tests for fully plastic fracture mechanics of plane strain mode I crack growth. In: Kirk, M., Bakker, A. (Eds.), Constraint Effects in Fracture: Theory and Applications, ASTM STP 1256. pp. 199–222.

Nyhus, B., Zhang, Z.L., Thaulow, C., 2002. Normalisation of material crack resistance curves by the *T*-stress. In: Proceedings of 14th European Conference on Fracture, September 8–13, 2002, Cracow, Poland.

Nyhus, B., Polanco, M.L., Ørjasæther, O., 2003. SENT specimens an alternative to SENB specimens for fracture mechanics testing of pipelines. In: Proceedings of OMAE03, 22nd International Conference in Offshore Mechanics and Arctic Engineering, June 8–13, 2003, Cancun, Mexico.

Østby, E., Jayadevan, K.R., Thaulow, C., 2005. Fracture response of pipelines subject to large plastic deformations under bending. International Journal of Pressure Vessels and Piping 82, 201–215.

Parks, D.M., 1981. The inelastic line-spring: estimates of elastic–plastic fracture mechanics parameters for surface cracked plates and shells. Transactions of the ASME, Journal of Pressure Vessel Technology 103, 246–254.

Parks, D.M., White, C.S., 1982. Elastic–plastic line-spring finite elements for surface-cracked plates and shells. Transactions of the ASME, Journal of Pressure Vessel Technology 104, 287–292.

Rice, J.R., 1972. The line-spring model for surface flaws. In: Swedlow, J.L. (Ed.), The Surface Crack: Physical Problems and Computational Solutions. American Society of Mechanical Engineers, New York, pp. 171–185.

Rice, J.R., Levy, N., 1972. The part-through surface crack in an elastic plate. Transactions of the ASME, Journal of Applied Mechanics 39, 185–194.

Sham, T.L., 1991. The determination of the elastic *T*-term using higher order weight functions. International Journal of Fracture 48, 81–102.

Sherry, A.H., France, C.C., Goldthorpe, M.R., 1995. Compendium of *T*-stress solutions for two and three dimensional cracked geometries. Fatigue and Fracture of Engineering Materials and Structures 18, 141–155.

Skallerud, B., 1999. Numerical analysis of cracked inelastic shells with large displacements for mixed mode loading. International Journal of Solids and Structures 36, 2259–2283.

Skallerud, B., Haugen, B., 1999. Collapse of thin shell structures–stress resultant plasticity modelling within a co-rotated ANDES finite element formulation. International Journal for Numerical Methods in Engineering 46, 1961–1986.

Skallerud, B., Holthe, K., Haugen, B., 2005. Thin shell and surface crack finite elements for simulation of combined failure modes. Computer Methods in Applied Mechanics and Engineering 194, 2619–2640.

Skallerud, B., Berg, E., Jayadevan, K.R., in press. Two-parameter fracture assessment of surface cracked cylindrical shells during collapse. Engineering Fracture Mechanics.

Storslett, L., 2004. Fracture Control Offshore Pipelines: Ductile crack growth of semi-elliptical surface cracks. Master's thesis, Norwegian University of Science and Technology, Norway (in Norwegian).

Tada, H., Paris, P.C., Irwin, G.R., 1985. The stress analysis of cracks handbook. Fracture Proof Design, Saint Louis, MO.

Thomason, P.F., 1990. Ductile Fracture of Metals. Pergamon Press Inc., Oxford.

Tvergaard, V., Needleman, A., 1984. Analysis of the cup-cone fracture in a round tensile bar. Acta Materiallia 32, 157–169.

Wang, Y.-Y., Parks, D.M., 1992. Evaluation of the elastic *T*-stress in surface-cracked plates using the line-spring method. International Journal of Fracture 56, 25–40.

Xia, L., Shih, C.F., 1995. Ductile crack growth—I. A numerical study using computational cells with microstructurally-based length scales. Journal of Mechanics and Physics of Solids 43, 233–259.

Zhang, Z.L., Thaulow, C., Ødegård, J., 2000. A complete Gurson model based approach for ductile fracture. Engineering Fracture Mechanics 67, 155–168.